Hydrothermal Synthesis and Oxygen Ionic Conductivity of Codoped Nanocrystalline $Ce_{1-x}M_xBi_{0.4}O_{2.6-x}$, M = Ca, Sr, and Ba

Hui Zhao and Shouhua Feng*

Key Laboratory of Inorganic Synthesis and Preparative Chemistry, Jilin University, Changchun 130023, People's Republic of China

Received August 21, 1998. Revised Manuscript Received November 23, 1998

A series of codoped nanocrystalline ceria compositions, $Ce_{1-x}M_xBi_{0.4}O_{2.6-x}$ (M = Ca, Sr, and Ba; $x = 0.01-0.15$) were hydrothermally synthesized at 240 °C and characterized by powder X-ray diffraction, transmission electron microscopy, and energy-dispersive X-ray spectroscopy. All as-made $Ce_{1-x}M_xBi_{0.4}O_{2.6-x}$ crystallize in cubic fluorite-type structures and exhibit solid solution properties. The average particle sizes of $Ce_{1-x}M_xBi_{0.4}O_{2.6-x}$ compositions obtained from hydrothermal systems were determined by the Scherrer equation and transmission electron microscopy to be approximately 32, 20, and 15 nm for Ca, Sr, and Ba systems, respectively. The oxygen ionic conductivities of the codoped $Ce_{1-x}M_xBi_{0.4}O_{2.6-x}$ were investigated by an ac (alternating current) impedance technique as a function of temperature and alkaline earth element contents. The highest ionic conductivity for $Ce_{0.95}Ca_{0.05}Bi_{0.4}O_{2.55}$ at 600 °C was 1.7×10^{-2} S·cm^{-1} with the activation energy $E_a = 46.3$ KJ·mol^{-1}. In addition, the ionic transference numbers for the Ca, Sr, and Ba codoped systems were almost unit, showing their highly pure ionic conductivities.

1. Introduction

It is well-known that CeO_2-based materials doped with aliovalent cations show promising ionic transport properties in application to solid oxide fuel cells and oxygen pumps.[1,2] Pure phase $CeO_{2-\delta}$ with cubic fluorite structure shows mixed electronic and ionic conduction,[3−5] and the introduction of lower-valence metal ions into the lattice of CeO_2 greatly improves their ionic conduction because of the quantitative formation of oxygen vacancies and in some cases eliminates its electronic conduction. Alkaline earth oxides such as CaO,[6−9] SrO,[10,11] and rare earth oxides Y_2O_3,[12,13] La_2O_3,[14] Gd_2O_3,[15−19] and Sm_2O_3[20−23] have been successfully used as dopants in the CeO_2-based systems to meet these requirements. Although the application temperature for CeO_2-based electrolytes was dramatically lowered and their conductivity was already higher than that for yttrium-stabilized zirconia (YSZ) or metal-doped ThO_2,[24] the enhancement and improvement of ionic conductivity of CeO_2-based materials for low-temperature applications still remain challenging.

All CeO_2-based systems studied to date are coupled with only one kind of aliovalent substitution (monodoped), for example, either divalent alkaline earth oxides or trivalent rare earth oxides. The motivation of this research is to look at codoped systems, for example, to introduce additional metal-ion dopants into the MO−CeO_2 systems, where M = Ca, Sr, and Ba. The selection of the second dopant, Bi^{3+} ions in this work, is based on such a fact that both CeO_2 and δ-Bi_2O_3 crystallize in fluorite-type structures, and CeO_2 exhibits large solubility for dopants such as CaO, SrO, Gd_2O_3, and La_2O_3.[25] The replacement of Ce^{4+} by Bi^{3+} could introduce oxygen vacancies, as expressed by the following reaction:

* To whom correspondence should be addressed.

(1) Subbarao, E. C.; Matti, H. S. *Solid State Ionics* **1981**, *5*, 539.
(2) Inaba, H.; Tagawa, H. *Solid State Ionics* **1996**, *83*, 1.
(3) Tuller, H. L.; Nowick, A. S. *J. Electrochem. Soc.* **1979**, *126*, 209.
(4) Blumenthal, R. N.; Hofmaier, R. L. *J. Electrochem. Soc.* **1974**, *121*, 126.
(5) Chang, E. K.; Blumenthal, R. N. *J. Solid State Chem.* **1988**, *72*, 330.
(6) Arai, H.; Kunisaki, T.; Shimizu, Y.; Seiyama, T. *Solid State Ionics* **1986**, *20*, 241.
(7) Garnier, J. E.; Blumenthal, R. N.; Panlener, R. J.; Sharma, R. K. *J. Phys. Chem. Solids* **1976**, *37*, 369.
(8) Blumenthal, R. N.; Pinz, B. A. *J. Appl. Phys.* **1976**, *38*, 2376.
(9) Eguchi, K.; Kunisaki, T.; Arai, H. *Commun. Am. Ceram. Soc.* **1986**, *69*, 282.
(10) Blumenthal, R. N.; Garnier, J. E. *J. Solid State Chem.* **1976**, *16*, 12.
(11) Yahiro, H.; Eguchi, K.; Arai, H. *Solid State Ionics* **1986**, *21*, 37.
(12) Wang, D. Y.; Nowick, A. S. *J. Solid State Chem.* **1980**, *35*, 325.
(13) Nowick, A. S.; Park, D. S. In *Superionic Conductors*; Mahanand, G. D., Roth, W. L., Eds.; Plenum: New York, 1976; p 395.
(14) Takahashi, T.; Iwahara, H. *Denki Kagaku* **1966**, *34*, 254.
(15) Kudo, T.; Obayashi, H. *J. Electrochem. Soc.* **1975**, *122*, 142.
(16) Kudo, T.; Obayashi, H. *J. Electrochem. Soc.* **1976**, *123*, 415.
(17) Eguchi, K.; Setoguchi, T.; Inoue, T.; Arai, H. *Solid State Ionics* **1992**, *52*, 165.
(18) Riess, T.; Braunshtein, D.; Tannhauser, D. S. *J. Am. Ceram. Soc.* **1981**, *64*, 479.
(19) Huang, K. Q.; Feng, M.; Goodenough, J. B. *J. Am. Ceram. Soc.* **1998**, *81*, 357.
(20) Gerhardt, R.; Nowick, A. S. *J. Am. Ceram. Soc.* **1986**, *69*, 641.
(21) Yahiro, H.; Eguchi, Y.; Eguchi, K.; Arai, H. *J. Appl. Electrochem.* **1988**, *18*, 527.
(22) Balazs, G. B.; Glass, R. S. *Solid State Ionics* **1995**, *76*, 155.
(23) Yamashita, K.; Ramanujachary, K. V.; Greenblatt, M. *Solid State Ionics* **1995**, *81*, 53.
(24) Badwal, S. P. S.; Foger, K. *Mater. Forum* **1997**, *21*, 187.
(25) Brauer, G.; Gradinger, H. *Z. Anorg. Allg. Chem.* **1954**, *276*, 209.

10.1021/cm980585k CCC: $18.00
Published on Web 03/13/1999

$$Bi_2O_3 \xrightarrow{CeO_2} 2Bi'_{Ce} + 3O_O + V_O^{\bullet\bullet}$$

where Bi'_{Ce} represents Bi^{3+} ions in Ce^{4+} sites, O_O represents O^{2-} ions on a regular oxygen lattice site, and $V_O^{\bullet\bullet}$ represents oxygen vacancies. The introduction of oxygen vacancies into a CeO_2 lattice may be expected to improve the ionic conductivity. According to Hund et al., the solubility of Bi_2O_3 in a CeO_2 sublattice was up to 40 molar %.[26] Furthermore, δ-Bi_2O_3-based material exhibited the highest oxygen ion conductivity among the fluorite structure materials at low temperature. Therefore, the codoping by both alkaline earth M^{2+} ions and Bi^{3+} ions simultaneously used as dopants in $Ce_{1-x}M_xBi_{0.4}O_{2.6-x}$ systems is expected to create low-temperature ionic conduction.

The synthesis and doping strategy were based on the hydrothermal technique. We have been making a lot of hydrothermal syntheses of complex oxides, fluorides, and hydrothermal doping as well, proving the hydrothermal technique to be a promising method.[27,28] Therefore, the application of hydrothermal techniques to the syntheses and doping of codoped ceria is expected. In addition, the hydrothermal synthesis facilitates a good control of the powder morphology by introduction of specific anions or surfactants and of the equilibrium incorporation of dopants into the powders in the early nucleation stage.[29−32] Yttrium-doped ceria solid electrolytes have been successfully produced by the hydrothermal method,[33] and the hydrothermal synthesis of solid electrolytes $Ce_{1-x}M_xO_{2-y}$ (M = Sm, Ca, Sr, Gd, and Y) has been recently studied by Greenblatt's group.[34,35] They found low-temperature ionic conductivities of 6×10^{-3} and 2×10^{-3} S·cm^{-1} at 600 °C for $Ce_{1-x}Sm_xO_{2-x/2}$ and $Ce_{1-x}Ca_xO_{2-x}$ systems, respectively.

In the present work, we report the hydrothermal syntheses and ionic conduction properties of a series of codoped nanocrystalline ceria, $Ce_{1-x}M_xBi_{0.4}O_{2.6-x}$ (M = Ca, Sr, and Ba; $x = 0.01-0.15$).

2. Experimental Section

Solid solutions $Ce_{1-x}M_xBi_{0.4}O_{2.6-x}$ were prepared by a hydrothermal method. Starting materials are $Ce(NO_3)_3 \cdot 6H_2O$, $Bi(NO_3)_3 \cdot 5H_2O$, $Ca(NO_3)_2 \cdot 4H_2O$, $Sr(NO_3)_2$, $Ba(NO_3)_2$, NaOH, and deionized water. The starting reaction compositions and reaction conditions are listed in Tables 1 and 2. A typical synthetic procedure for $Ce_{0.9}Ba_{0.1}Bi_{0.4}O_{2.5}$ is described as follows: 0.415 g of cerium(III) nitrate hexahydrate, 0.194 g of bismuth(III) nitrate pentahydrate, and 0.013 g of $Ba(NO_3)_2$ were dissolved into 8 mL of deionized water to form a solution, to which 2 mL of 2.5 M NaOH was added dropwise with stirring to form a dark yellowish suspension. The mole composition of the final reaction mixture was $1.00CeO_2/0.42Bi_2O_3/0.05BaO/580H_2O/2.60Na_2O$. The mixture was sealed into Teflon-lined stainless steel autoclaves and crystallized at 240 °C for 24 h. The final products were filtered, washed with deionized water, and dried at room temperature. All other syntheses have similar procedures mentioned above, but alternating starting materials were employed according to corresponding codoping systems.

Table 1. Typical Starting Reactant Mole Ratios and Composition of Final Products

nominal mole ratio of starting materials	mole ratios of final products	product fomula $Ce_{1-x}M_xBi_{0.4}O_{2.6-x}$
Ce:Ca:Bi	Ce:Ca:Bi	
0.97:0.03:0.40	0.969:0.031:0.41	$Ce_{0.97}Ca_{0.03}Bi_{0.4}O_{2.57}$
0.95:0.05:0.40	0.951:0.049:0.40	$Ce_{0.95}Ca_{0.05}Bi_{0.4}O_{2.55}$
0.90:0.10:0.40	0.898:0.101:0.41	$Ce_{0.90}Ca_{0.10}Bi_{0.4}O_{2.50}$
0.85:0.15:0.40	0.851:0.148:0.41	$Ce_{0.85}Ca_{0.15}Bi_{0.4}O_{2.45}$
0.83:0.17:0.40	0.848:0.152:0.40	$Ce_{0.85}Ca_{0.15}Bi_{0.4}O_{2.45}$
0.80:0.20:0.40	0.852:0.148:0.40	$Ce_{0.85}Ca_{0.15}Bi_{0.4}O_{2.45}$
Ce:Sr:Bi	Ce:Sr:Bi	
0.99:0.01:0.40	0.987:0.013:0.405	$Ce_{0.99}Sr_{0.01}Bi_{0.4}O_{2.59}$
0.97:0.03:0.40	0.971:0.029:0.402	$Ce_{0.97}Sr_{0.03}Bi_{0.4}O_{2.57}$
0.92:0.08:0.40	0.918:0.082:0.400	$Ce_{0.92}Sr_{0.08}Bi_{0.4}O_{2.52}$
0.89:0.11:0.40	0.889:0.110:0.407	$Ce_{0.89}Sr_{0.11}Bi_{0.4}O_{2.49}$
0.85:0.15:0.40	0.902:0.098:0.401	$Ce_{0.90}Sr_{0.10}Bi_{0.4}O_{2.50}$
Ce:Ba:Bi	Ce:Ba:Bi	
0.99:0.01:0.40	0.991:0.009:0.401	$Ce_{0.99}Ba_{0.01}Bi_{0.4}O_{2.59}$
0.97:0.03:0.40	0.969:0.031:0.402	$Ce_{0.97}Ba_{0.03}Bi_{0.4}O_{2.57}$
0.92:0.08:0.40	0.922:0.078:0.399	$Ce_{0.92}Ba_{0.08}Bi_{0.4}O_{2.52}$
0.90:0.10:0.40	0.901:0.099:0.400	$Ce_{0.90}Ba_{0.10}Bi_{0.4}O_{2.50}$
0.85:0.15:0.40	0.897:0.103:0.401	$Ce_{0.90}Ba_{0.10}Bi_{0.4}O_{2.50}$

Table 2. Effects of Bismuth Precursor on the Formation of $Ce_{1-x}M_xBi_{0.4}O_{2.6-x}$

bismuth precursor	reaction temp (°C)	reaction time (h)	product phases
$BiCl_3$	180	24	γ-$Bi_2O_3 + CeO_2$
$BiCl_3$	240	6	γ-$Bi_2O_3 + CeO_2$
$BiCl_3$	240	12	CBC[a]
$BiCl_3$	240	24	CBC
$Bi(NO_3)_3$	180	24	α-$Bi_2O_3 + CeO_2$
$Bi(NO_3)_3$	240	6	γ-$Bi_2O_3 + CeO_2$
$Bi(NO_3)_3$	240	12	CBC
$Bi(NO_3)_3$	240	24	CBC
$NaBiO_3$	160	24	α-$Bi_2O_3 + CeO_2$
$NaBiO_3$	180	24	α-$Bi_2O_3 + CeO_2$
$NaBiO_3$	240	12	γ-$Bi_2O_3 + CeO_2$
$NaBiO_3$	240	24	α-$Bi_2O_3 + CeO_2$

[a] CBC represents $Ce_{1-x}M_xBi_{0.4}O_{2.6-x}$, M = Ca, Sr, and Ba.

Powder X-ray diffraction (XRD) was determined by a Rigaku, *D*/max-rA diffractometer with Ni-filtered CuKα radiation at room temperature. The scan rate was 0.1° 2θ min^{-1}. Silicon powder was used as an internal standard and the lattice parameters were refined by least-squares methods. The average grain sizes (*D*) were determined from the XRD patterns using the Scherrer equation,[36] $D = 0.9\lambda/\beta \cos\theta$ where λ, β, and θ have normal meanings, and by an H-8100 transmission electron microscope (TEM) equipped with an energy disperse X-ray spectrometer (EDX) analyzer. EDX was used to determine the composition of the products.

In electrical measurements, powder samples were pressed into a compact (10 mm in diameter and 3 mm in thickness) under 35 MPa. The disk was sintered at 1000 °C for 8 h in air. The sintered samples were over 92% of the theoretical density determined by a water pycnometric technique. The

(26) Hund, F. *Z. Anorg. Allg. Chem*. **1964**, *333*, 248.
(27) (a) Feng, S.; Greenblatt, M. *Chem. Mater.* **1992**, *4*, 462. (b) Feng, S.; Greenblatt, M. *Chem. Mater*. **1993**, *5*, 1277. (c) Feng, S.; Tsai, M.; Shi, S.; Greenblatt, M. *Chem. Mater*. **1992**, *4*, 468.
(28) (a) Zhao, C.; Feng, S.; Chao, Z.; Shi, C.; Xu, R.; Ni, J. *Chem. Commun*. **1996**, 1641. (b) Xun, X.; Feng, S.; Wang, J.; and Xu, R. *Chem. Mater*. **1997**, *9*, 2966. (c) Xun, X.; Feng, S.; Xu, R. *Mater. Res. Bull*. **1998**, *33* (3), 369.
(29) Somiya, S.; Yoshimura, M.; Nakai, Z.; Hishinuma, K.; Kumaki, T. *Adv. Ceram*. **1987**, *21*, 43.
(30) (a) Zhao, C.; Feng, S.; Chao, Z.; Shi, C.; Xu, R.; Ni, J. *Chem. Commun*. **1997**, 945. (b) Pang, G.; Feng, S.; Gao, Z.; Xu, Y.; Zhao, C.; and Xu, R. *J. Solid State Chem*. **1997**, *128* (2), 313.
(31) Li, G.; Feng, S.; Li, L.; Li, X.; Jin, W. *Chem. Mater*. **1997**, *9*, 2894.
(32) Komarneni, S.; Fregeau, E.; Breval, E.; Roy, R. *J. Am. Ceram. Soc*. **1988**, *C26*, 71.
(33) Zhou, Y. C.; Rahaman, M. N. *J. Mater. Res*. **1993**, *8*, 1680.
(34) Yamashita, K.; Ramanujachary, K. V.; Greenblatt, M. *Solid State Ionics* **1995**, *81*, 53.
(35) Huang, W.; Shuk, P.; Greenblatt, M. *Chem. Mater*. **1997**, *9*, 2240.
(36) Mitoff, S. P. *J. Chem. Phys*. **1962**, *36*, 1383.

electrical conductivity of the sintered disk was measured under different atmospheres: oxygen, air, nitrogen, and helium. The water content in the gas (nitrogen stream) was fixed by mixing a part of the gas saturated with water at 20 °C with a part dried over P_2O_5. Platinum paste was painted on two sides of the disk as electrodes, and the disk with electrodes was sintered again at 800 °C for 30 min to erase the solvent. The ionic conductivity measurements were performed by an ac (alternating current) complex impedance method at frequencies ranging from 0.1 to 1 MHz on a Solartron 1260 impedance/gain-phase analyzer. The dc (direct current) resistance measurement was conducted on a Solartron 1287 electrochemical interface. The current that appeared by applying the constant voltage (10 mV) on the two Pt electrodes was monitored as a function of time. The dc conductivity (σ_{dc}) was calculated by the applied voltage, the generated current, the surface area of the Pt electrode, and the thickness of the pellet. As Pt was not a completely blocking electrode for oxygen ions, the ionic transference number (t_i) was estimated from the polarization data measured in helium. As we know, $t_i = \sigma_i/\sigma_t = \sigma_i/\sigma_i + \sigma_e$, where σ_i, σ_t, and σ_e are the ionic, total, and electronic conductivity, respectively.[36] In terms of dc conductivity of codoped ceria, it can be written as $(\sigma_{dc})_{t=0} = \sigma_t = \sigma_i + \sigma_e$ and $(\sigma_{dc})_{t=\infty} = \sigma_i' + \sigma_e$, where t refers to the time scale of the measurement and σ_i' refers to the rest current caused by oxygen ions. When the measurement was conducted in helium, the value of σ_i' would be very low compared to that of σ_e. As a whole, the ionic transference number can be determined by $t_i = \sigma_i/\sigma_t = 1 - (\sigma_{dc})_{t=\infty}/(\sigma_{dc})_{t=0}$.

3. Results and Discussion

3.1. Hydrothermal Synthesis. The starting reaction composition is a major factor for determining the formation of a pure codoped compound. Table 1 lists typical starting reactant mole ratios and composition of final products for the syntheses of $Ce_{1-x}M_xBi_{0.4}O_{2.6-x}$. The composition of final products was closely related to their corresponding starting reactant composition in the range of x values, 0.01−0.15 for the Ca system and 0.01−0.10 for the Sr and Ba systems. The final molar ratios of Ce, Bi, and M quantitatively determined by EDX as listed in Table 1 are almost equal to the nominal ones when $x < 0.15$, but deviations when $x > 0.15$ were clearly observed for the Ca system, for $x > 0.10$ for the Sr system, and for $x > 0.10$ for the Ba systems, respectively, due to their solubility limits at these points.

Different reactants were used as starting materials in this work. The type of starting materials dramatically affected the formation of final products. Pure phase solid solution of $Ce_{1-x}M_xBi_{0.4}O_{2.6-x}$ could be obtained when $Bi(NO_3)_3{\cdot}6H_2O$ or $BiCl_3$ were used as the Bi precursor, whereas when $NaBiO_3$ was used as a starting material, α-Bi_2O_3 was obtained in most cases as a major phase in the final product (see Table 2). The same phenomenon was also obtained by Kinomura et al.[39] when they prepared bismuth oxides such as Bi_2O_4 in a hydrothermal system.

The reaction temperature also dominated the formation of the codoped CeO_2-based solid solution. Lower reaction temperatures such as <200 °C led to the formation of mixed oxides of α-Bi_2O_3 (in some cases γ-Bi_2O_3) and CeO_2. Thus, the reaction temperature greater than 200 °C was critical for preparing pure products. The reaction time associated with reaction temperature affected the formation and purity of final products. When the reaction time was less than 6 h, α-Bi_2O_3 and unreacted $Ce(OH)_3{\cdot}xH_2O$ were found, whereas with reaction times to 12 h, the $Ce_{1-x}M_xBi_{0.4}O_{2.6-x}$ could be formed and well-crystallized after an additional 12 h in all systems.

3.2. Phases and Morphology. Figure 1a−c show XRD patterns of $Ce_{1-x}M_xBi_{0.4}O_{2.6-x}$, M = Ca, Sr, and Ba hydrothermally synthesized at 240 °C for 24 h with selected M contents x. All codoped ceria samples with x values $0.01 < x < 0.15$ have cubic fluorite structures for their XRD patterns which are similar to that of pure CeO_2 with the cubic fluorite structure. Some slight shifts in diffraction angles were found in different systems, because of the dissolution of the dopants MO and Bi_2O_3 into the CeO_2 fluorite structures. It was clearly seen that all cell parameters of $Ce_{1-x}M_xBi_{0.4}O_{2.6-x}$ increased initially with increasing M contents, as shown in Figure 2, and became constant at $x = 0.15$ for the Ca system, at $x = 0.11$ for the Sr system, and at $x = 0.10$ for the Ba system, respectively. Beyond the x values, impurities were found for each system (as shown in Figure 1b; for the specific Sr system with $x = 0.11$, prolonging the reaction time such as 30 h results in a pure product and its XRD pattern is shown). This result is consistent with the effect of doping ion size, for example, both divalent alkaline earth ions ($r_{M(II)} \sim 0.116$ nm) and trivalent bismuth ions ($r_{Bi(III)} = 0.120$ nm) are bigger than tetravalent cerium ions ($r_{Ce(IV)} = 0.101$ nm). The limiting x value for each system reflects the similarity of M^{2+} ions to Ce^{4+} ions in size such as the radii of Ca^{2+}, Sr^{2+}, and Ba^{2+} being 0.112, 0.125, and 0.142 nm, respectively. This was confirmed by their composition analysis (see Table 1).

EDX was employed to detect if the mineralizer NaOH was incorporated into the final products. Figure 3 shows a typical EDX spectrum of a codoped Ca system. There are no emission peaks at about 1.04 keV, characteristic for sodium atoms, indicating no evidence for sodium in the final products, although the syntheses proceed in a NaOH solution.

The broadening effects in XRD patterns of hydrothermally synthesized products were observed. The mean particle sizes for all $Ce_{1-x}M_xBi_{0.4}O_{2.6-x}$ obtained from the Scherrer equation are ∼32, ∼20, and ∼15 nm for the Ca, Sr, and Ba systems, respectively. It was found that the particle sizes decreased linearly in the order of Ca, Sr, and Ba at the same x value. This can be explained in part by the effects of doping ion radii. The size of calcium ions, similar to that of cerium ions, is much better matched in the ceria lattice than that of the barium ion, and thus the Ca system may have relative priority in the course of crystal growth compared to the Ba system. The TEM image for the Ca system (see Figure 4) also proved that the particles are of nanosize. The mean particle size measured from TEM is consistent with the result from the Scherrer estimation.

3.3. Electrical Conductivity. Alternating current (ac) impedance measurements of $Ce_{1-x}M_xBi_{0.4}O_{2.6-x}$ were performed in air in the temperature range of 300−600 °C. A typical complex impedance plot for $Ce_{1-x}M_xBi_{0.4}O_{2.6-x}$ resolved the bulk, grain-boundary,

(37) Kilner, J. A.; Steele, B. C. H. In *Nonstoichiometric Oxides*; Toft Sørensen, O., Ed.; Academic: New York, 1981.
(38) Takahashi, T. In *Physics of Electrolyte*; Ladik, J. H., Ed.; Academic: New York, 1972; p 989.
(39) Kinomura, N.; Kumada, N. *Mater. Res. Bull.* **1995**, *30*, 129.

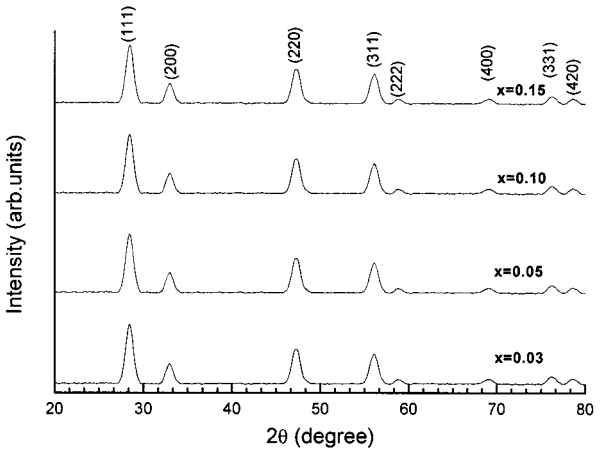

(a) $Ce_{1-x}Ca_xBi_{0.4}O_{2.6-x}$

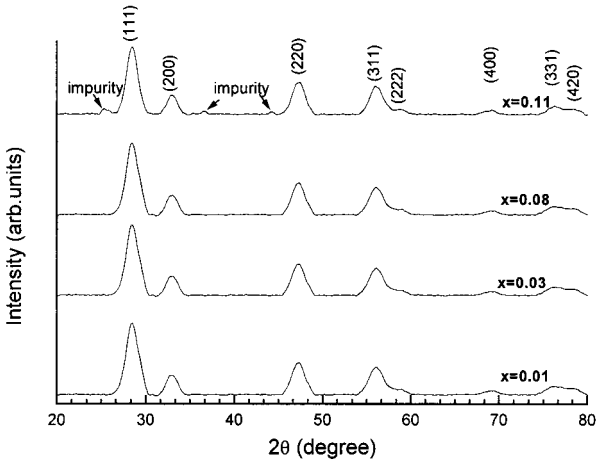

(b) $Ce_{1-x}Sr_xBi_{0.4}O_{2.6-x}$

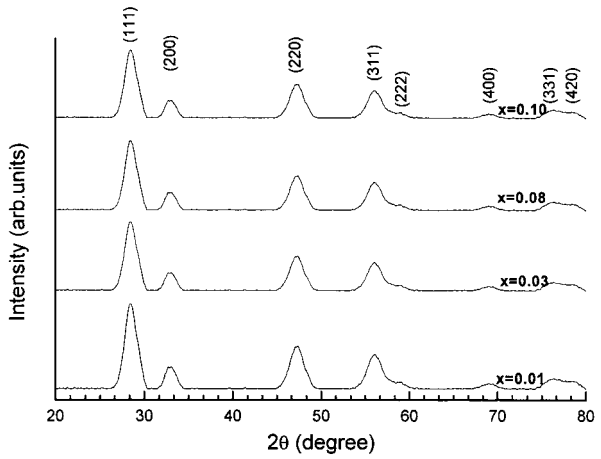

(c) $Ce_{1-x}Ba_xBi_{0.4}O_{2.6-x}$

Figure 1. XRD patterns of (a) $Ce_{1-x}Ca_xBi_{0.4}O_{2.6-x}$ with x = 0.03, 0.05, 0.10, and 0.15; (b) $Ce_{1-x}Sr_xBi_{0.4}O_{2.6-x}$ with x = 0.01, 0.03, 0.08, and 0.11; (c) $Ce_{1-x}Ba_xBi_{0.4}O_{2.6-x}$ with x = 0.01, 0.03, 0.08, and 0.10.

and electrode con-ductionprocesses by exhibiting successive semicircles in the complex plane. In the case of $Ce_{0.95}Ca_{0.05}Bi_{0.4}O_{2.55}$, the responses that were separated into contributions from the grains, grain-boundaries, and electrode processes are indicated in Figure 5. It can be seen that the bulk and grain-boundary processes remain distinguishable at 600 °C, and that the grain semicircle is incomplete, indicating that the time constant of the grain response is too short even at 600 °C. Overall ionic conductivity was determined from the reciprocal of resistivity at the right-side intercept of the grain-boundary semicircular arc with the Z' axis of the $Z'-Z''$ plot.

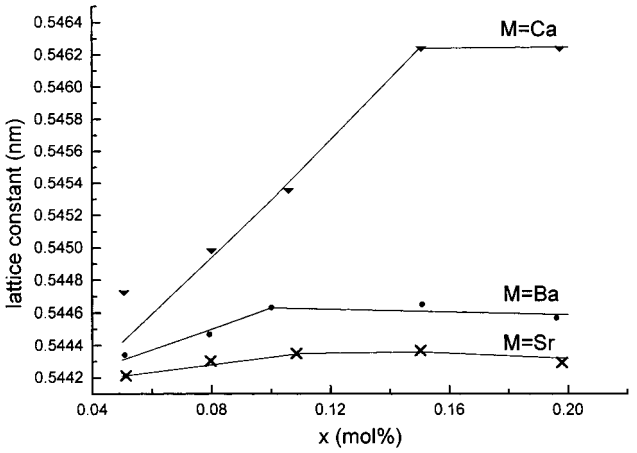

Figure 2. Relationship of cell parameters of $Ce_{1-x}M_xBi_{0.4}O_{2.6-x}$ with M content x.

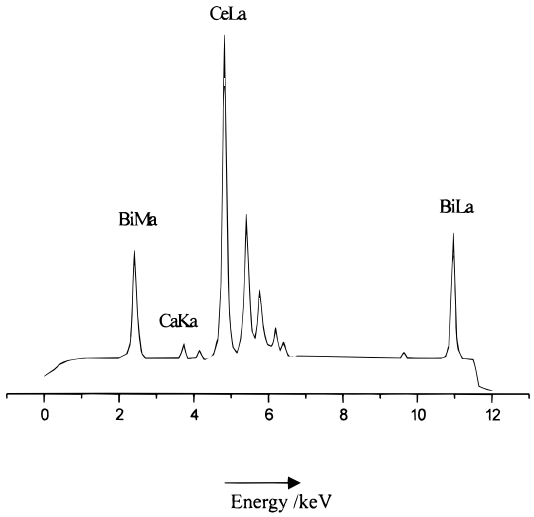

Figure 3. EDX spectrum of $Ce_{0.95}Ca_{0.05}Bi_{0.4}O_{2.55}$.

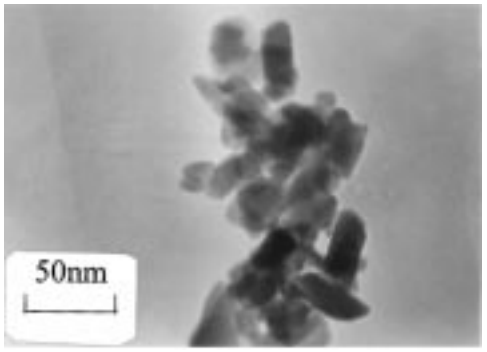

Figure 4. TEM of $Ce_{0.95}Ca_{0.05}Bi_{0.4}O_{2.55}$.

The Arrhenius plots of the ionic conductivity of $Ce_{1-x}M_xBi_{0.4}O_{2.6-x}$, M = Ca, Sr, and Ba, are shown in Figure 6a–c. Straight lines are obtained from 300 to 600 °C without discontinuity and the relatively similar values of activation energies for ionic conduction in each system (ca. 48.9, 67.2, and 57.3 KJ·mol^{-1} for Ca, Sr, and Ba systems, respectively) imply a single conduction mechanism for these systems. In each system, activation

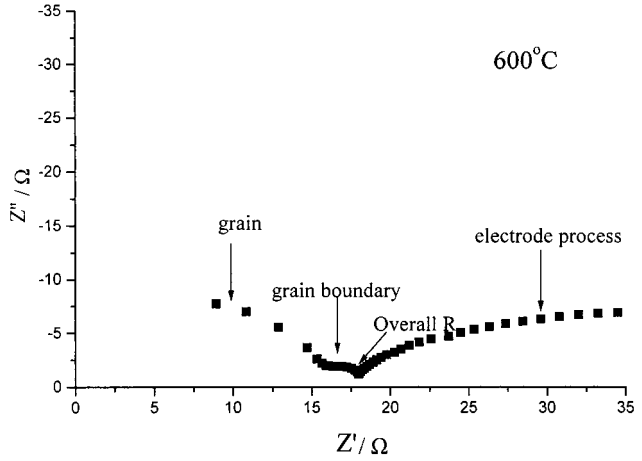

Figure 5. Impedance plot of $Ce_{0.95}Ca_{0.05}Bi_{0.4}O_{2.55}$ at 600 °C.

Table 3. Cell Parameters, Particle Sizes, and Conductivity Data for $Ce_{1-x}M_xBi_{0.4}O_{2.6-x}$

$Ce_{1-x}M_x$-$Bi_{0.4}O_{2.6-x}$	*a* (nm)	*D*[a] (nm)	$\sigma_{600°C}$ ($S\cdot cm^{-1}$)	E_a ($KJ\cdot mol^{-1}$)	t_i[b]
M = Ca					
$x = 0.03$	0.5447(3)	27.3(3)	$8.9(5) \times 10^{-3}$	50.4(5)	0.99
$x = 0.05$	0.5452(2)	30.6(4)	$1.7(2) \times 10^{-2}$	46.3(4)	0.99
$x = 0.10$	0.5462(5)	36.1(6)	$2.1(4) \times 10^{-3}$	48.8(2)	0.99
$x = 0.15$	0.5461(8)	37.4(3)	$4.5(1) \times 10^{-3}$	50.1(4)	0.99
M = Sr					
$x = 0.01$	0.5442(2)	11.9(4)	$5.3(6) \times 10^{-3}$	75.8(2)	0.99
$x = 0.03$	0.5443(2)	13.5(5)	$7.4(4) \times 10^{-3}$	59.9(1)	0.99
$x = 0.08$	0.5443(6)	13.7(4)	$2.1(7) \times 10^{-3}$	57.3(1)	0.99
$x = 0.11$	0.5443(1)	14.2(3)	$4.6(3) \times 10^{-3}$	75.7(5)	0.99
M = Ba					
$x = 0.01$	0.5443(5)	14.3(1)	$2.8(2) \times 10^{-3}$	62.1(6)	0.89
$x = 0.03$	0.5446(4)	17.1(5)	$4.5(6) \times 10^{-3}$	53.6(6)	0.92
$x = 0.08$	0.5446(6)	14.9(3)	$3.7(3) \times 10^{-3}$	53.3(8)	0.90
$x = 0.10$	0.5445(8)	15.1(2)	$3.5(5) \times 10^{-3}$	60.3(4)	0.91

[a] *D*: average grain size. [b] t_i: ionic transference number.

energies E_a (see Table 3) decreased linearly with increasing M contents. For the Ca codoped system, E_a had a minimum at $x = 0.05$ and then increased sharply with increasing M content. This phenomenon, applying to all three systems, can be attributed to the formation of oxygen vacancy associates $\{Ca''_{Ce}V^{\bullet\bullet}_O\}$ in the fluorite structure, for example, the number of oxygen vacancies increased linearly with increasing Ca content and reached a maximum at $x = 0.05$. Beyond the maximum value of *x*, the defect associates $\{Ca''_{Ce}V^{\bullet\bullet}_O\}$ formed, lead to a decrease of oxygen vacancy concentration, and thus increase the activation energy.[37]

The highest ionic conductivity, $\sigma_{600°C} = 1.7 \times 10^{-2}$ $S\cdot cm^{-1}$, was found in $Ce_{0.95}Ca_{0.05}Bi_{0.4}O_{2.55}$, which is almost 1 order of magnitude higher than that of CaO-stabilized ZrO_2.[38] This value was also much higher than that of calcium-doped ceria (2×10^{-3} $S\cdot cm^{-1}$).[35] It is also noted that the ionic conductivity of the Ba-substituted ceria system reported by Yahiro et al.[40] is about 2 orders of magnitude lower than that of the Ca-substituted system. But in our codoped systems studied here, the ionic conductivity of the Ba codoped system was dramatically improved, reaching that of the Ca and the Sr codoped systems.

To understand the ionic transference numbers of the $Ce_{1-x}M_xBi_{0.4}O_{2.6-x}$ codoped systems, the dc conductivity of the Ca codoped system was measured as a function of time. Figure 7 shows the time dependence of the dc

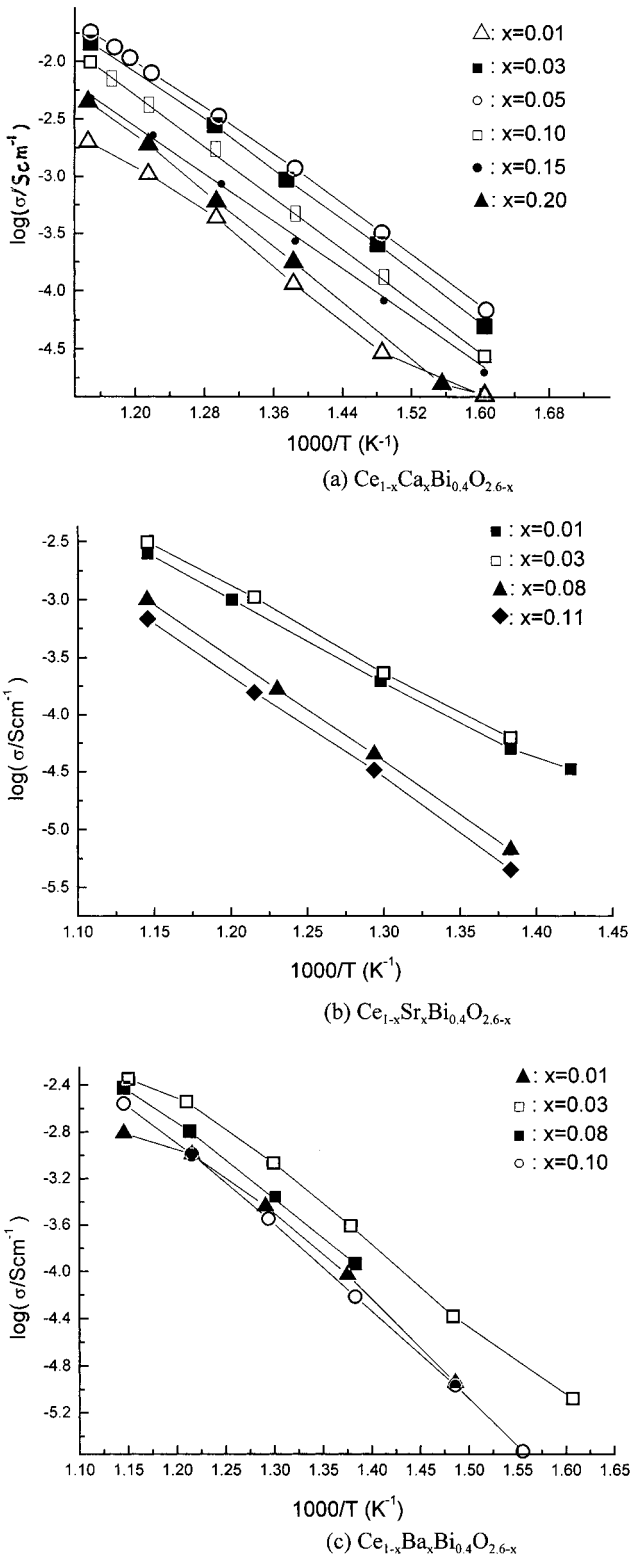

Figure 6. Arrhenius plots of ionic conductivity of (a) $Ce_{1-x}Ca_xBi_{0.4}O_{2.6-x}$, (b) $Ce_{1-x}Sr_xBi_{0.4}O_{2.6-x}$, and (c) $Ce_{1-x}Ba_x$-$Bi_{0.4}O_{2.6-x}$.

conductivity of $Ce_{0.95}Ca_{0.05}Bi_{0.4}O_{2.55}$ at 600 °C in different atmospheres (oxygen, air, nitrogen, and helium). The dc conductivity decreased abruptly in comparison to its ac conductivity and finally approached a steady value. The ionic transference number t_i of codoped CeO_2-

(40) Yahio, H.; Ohuchi, T.; Eguchi, K.; Arai, H. *J. Mater. Sci.* **1988**, *23*, 1036.

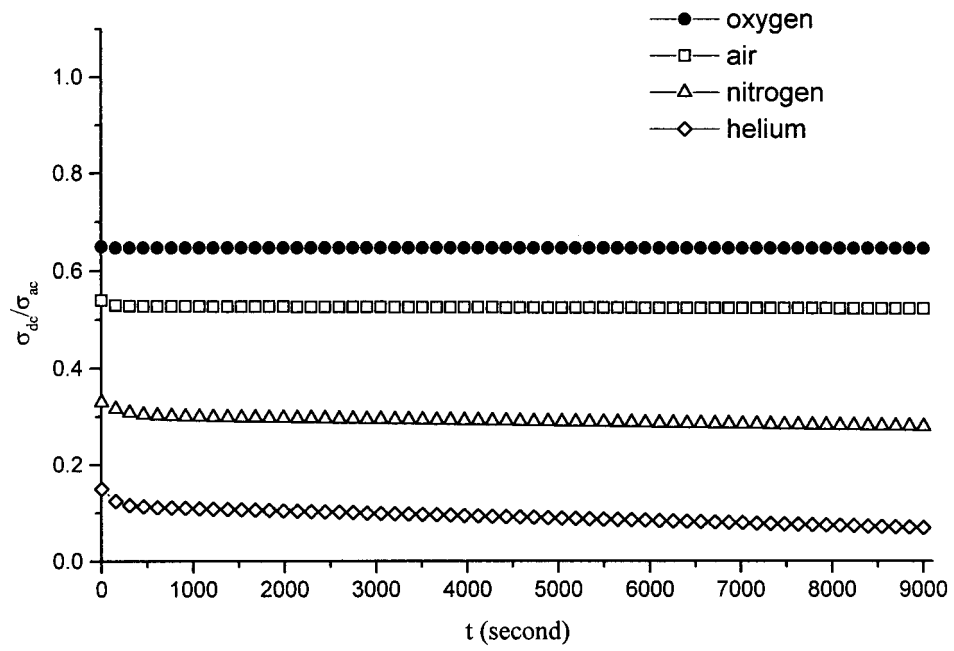

Figure 7. Direct current (dc) conductivity of $Ce_{0.95}Ca_{0.05}Bi_{0.4}O_{2.55}$ at 600 °C in different atmospheres (oxygen, air, nitrogen, and helium) as a function of time.

based oxides was estimated from the dc polarization results measured in helium (see Table 3). The ionic transference number of undoped CeO_2 is only 0.4, whereas those of the Ca and Sr codoped systems are almost unit. For the Ba codoped system, $t_i > 0.90$ is obtained in a wide range of M ion concentrations. On the basis of the fact that in the monodoped $BaO-CeO_2$ system t_i only ranges between 0.5 and 0.8,[40] our current codoping of the ceria systems dramatically improved the ionic conductivity and suppressed the electronic conductivity.

From Figure 7 we also noted that the polarization behavior increased with the decrease of oxygen pressure. Furthermore, the dc and ac conductivity ratio of (σ_{dc}/σ_{ac}) was not unit, even though the measurement was conducted in oxygen. The result was different from that of well-known oxygen ions conductor HfO_2[41] and indicated that, besides the oxygen ions conduction, there should exist some other conduction species.

To identify the conduction species, the conductivity of the codoped system was measured in a different water partial pressure. The result was shown in Figure 8. The conductivity increased with increasing the water vapor pressure and a linear relationship could be obtained in such a situation. This therefore proved that proton conduction exists in the hydrothermal synthesized compounds. The reason for proton conduction was not clear. Perhaps the rest water that exists in the hydrothermally produced ceria compounds has anticipated the conduction at higher temperature. An absorption band at about 3700 cm^{-1} in the IR spectrum[42] also proved the existing of rest water (Figure 9).

To investigate the influence of the gas atmosphere over the codoped samples on their conductivity, oxygen, nitrogen, and air were introduced into the measuring system. It was observed that the oxygen gas had a

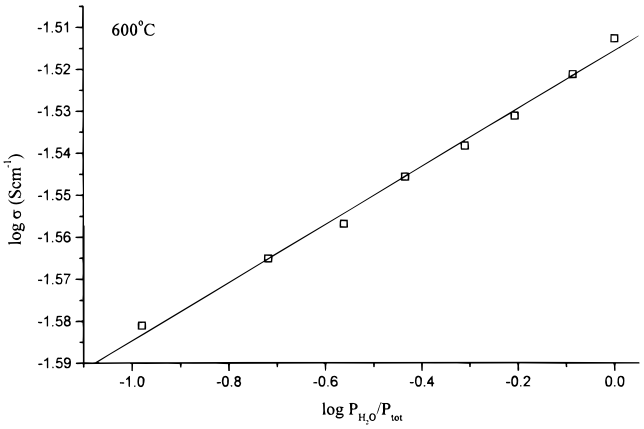

Figure 8. Alternating current (ac) conductivity of $Ce_{0.95}Ca_{0.05}Bi_{0.4}O_{2.55}$ at 600 °C as a function of water partial pressure.

dramatic influence on the low-frequency electrode response, but had no effects on the grain and grain-boundary conductivity, as shown in Figure 10. This result shows that no electron conduction exists in the codoped system; the main conduction is ionic. In flowing N_2, the low-frequency response consists of an inclined spike at an angle of ca. 45°, but in air or in flowing oxygen, a suppressed semicircle arc could be observed. Such an observation indicates that a Warburg-like response exists at low frequencies, which can be ascribed to ambipolar drag of one set of charges on the other set, when proton and oxygen ions have different mobilities in the codoped cerias.[43] All these results therefore show that a mixed proton and oxygen ionic conductor has been produced by our hydrothermal method.

(41) Kobayashi, Y.; Egawa, T.; Tamura, S.; Imanaka, N.; Adachi, G.-Y. *Chem. Mater.* **1997**, *9*, 1649.

(42) Nyquist, R. A.; Kagel, R. O. *Infrared Spectra of Inorganic Compounds*; Academic Press: New York, 1971.

(43) (a) Macdonald, J. R. *J. Electroanal. Chem.* **1971**, *32*, 317. (b) Macdonald, J. R. *J. Electroanal. Chem.* **1974**, *53*, 1. (c) Franceschetti, D. R.; Macdonald, J. R. *J. Electroanal. Chem.* **1979**, *101*, 307. (d) Armstrong, R. D.; Bell, M. F.; Metcalfe, A. A. In *Electrochemistry*; Specialist Periodical Report; Thirsk, H. R., Senior Reporter; The Chemical Society: London, 1978; Vol. 6, p 98. (e) Macdonald, J. R.; Hull, C. A. *J. Electroanal. Chem.* **1984**, *165*, 9.

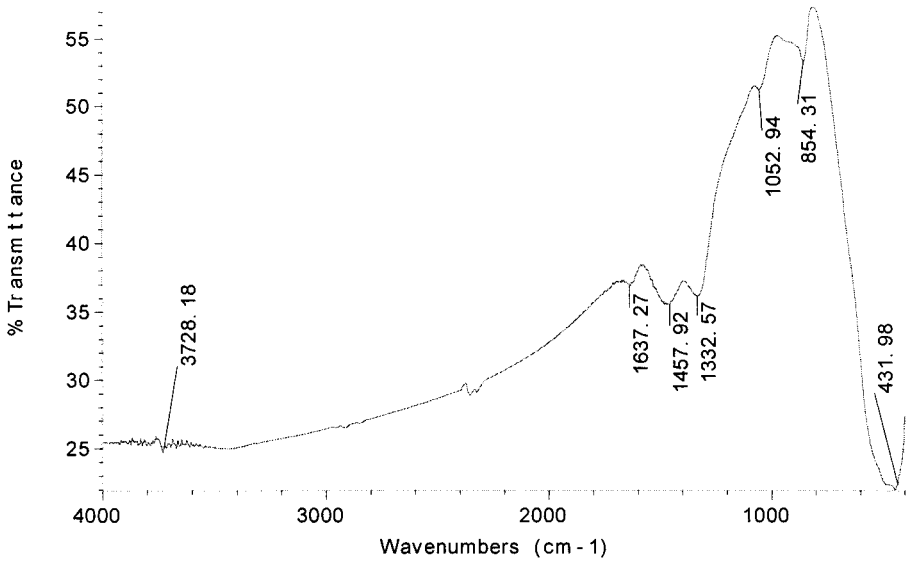

Figure 9. IR spectrum of $Ce_{0.95}Ca_{0.05}Bi_{0.4}O_{2.55}$.

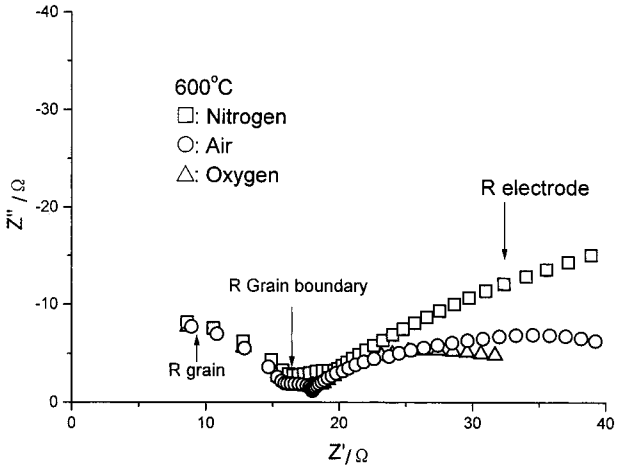

Figure 10. Impedance plots of $Ce_{0.9}Ca_{0.1}Bi_{0.4}O_{2.5}$ measured at 600 °C in nitrogen, air, and oxygen.

4. Conclusions

A series of codoped ceria solid solutions, $Ce_{1-x}M_xBi_{0.4}O_{2.6-x}$ (M = Ca, Sr, and Ba) have been successfully synthesized by a hydrothermal method at 240 °C for 24 h. The particle sizes of all samples were in the nanometer range because of the use of a hydrothermal synthesis technique. The ionic conductivity has been greatly enhanced in these codoped systems. The highest ionic conductivity for $Ce_{0.95}Ca_{0.05}Bi_{0.4}O_{2.55}$ at 600 °C was 1.7×10^{-2} S·cm^{-1}, which was much higher than that of well-known Ca-stabilized zirconia and calcium monodoped ceria. For the barium codoped system, both the ionic conductivity and ionic transference number have been improved. The current codoped nanocrystalline $Ce_{1-x}M_xBi_{0.4}O_{2.6-x}$ show the mixed proton and oxygen ionic conduction and belong to one of the best ionic conductors.

Acknowledgment. This work was supported by NSFC through the project of Inorganic Synthesis Chemistry No. 29731010.

CM980585K